KICSP 한국 융합신호처리학회

융합신호처리학회논문지 Vol. 24, No. 1 : 1~14 March. 2023
DOI : 10.23087/jkicsp.2023.24.1.001

Underwater Optical Image Data Transmission in the Presence of Turbulence and Attenuation

Ramavath Prasad Naik[1], Maaz Salman[1], Wan-Young Chung[2*]

[1]Department of Artificial Intelligence and Convergence, Pukyong national university
[2]Department of Electronic Engineering, Pukyong national university

Abstract Underwater images carry information that is useful in the fields of aquaculture, underwater military security, navigation, transportation, and so on. In this research, we transmitted an underwater image through various underwater mediums in the presence of underwater turbulence and beam attenuation effects using a high-speed visible optical carrier signal. The optical beam undergoes scintillation because of the turbulence and attenuation effects; therefore, distorted images were observed at the receiver end. To understand the behavior of the communication media, we obtained the bit error rate (BER) performance of the system with respect to the average signal-to-noise ratio (SNR). Also, the structural similarity index (SSI) and peak SNR (PSNR) metrics of the received image were evaluated. Based on the received images, we employed suitable nonlinear filters to recover the distorted images and enhance them further. The BER, SSI, and PSNR metrics of the specific nonlinear filters were also evaluated and compared with the unfiltered metrics. These metrics were evaluated using the on-off keying and binary phase-shift keying modulation techniques for the 50-m and 100-m links for beam attenuation resulting from pure seawater, clear ocean water, and coastal ocean water mediums.

• Key Words : Underwater image, bit error rate, peak signal to noise ratio, structural similarity index, non-linear filter.

Received 11 January 2023, Revised 08 February 2023, Accepted 10 February 2023

*** Corresponding Author** Wan-Young Chung, Department of Electronic Engineering, Pukyong national university, Busan 48513, Korea. E-mail: wychung@pknu.ac.kr

Ⅰ. INTRODUCTION

Two-thirds of earth's surface is covered with the water; the oceans and seas account for most of the water on the earth. Underwater environments provide many benefits, such as transportation, food, recreation, minerals, and climate control [1]. In addition, underwater environments are used for military services; anti-submarine warfare is used to track, detect, damage, or destroy enemy submarines [2]. However, because of the hostile nature of the underwater environments, a large portion of the underwater environment remains unexplored. The study and monitoring of unexplored underwater environments can help reveal these environments from the shore. However, for high speeds, an efficient communication scheme needs to be enabled. Radio frequency (RF) signals are restricted because of the high attenuation in underwater mediums [3]. Acoustic signals have lower transmission speeds, multipath propagation, and high latency [4]. The optical carrier can be an alternative to RF signals and acoustics, which can transmit with higher transmission speeds with less beam attenuation for the medium-range links [5].

Underwater images carry the exact information that needs to be conveyed rather than transmitting only the data. However, underwater images suffer from color distortion, contrast degradation and poor visibility due to the optical beam absorption and scattering effects. In addition to these effects underwater turbulence during the optical data transmission causes fading of colors increases with increase in water depth, the objects at a distance of more-than 10 meters from the water surface are harder to distinguish [6,7]. Beam attenuation is an additive quantity of absorption and scattering [8]. Beam absorption arises because of the chlorophyll content present in green plants, which traps the light to provide energy for photosynthesis. Beam scattering arises because of the presence of suspended particles in the underwater medium, which changes the direction of the optical beams. The magnitudes of absorption and scattering vary based on the variations in the water types [9]. These factors motivated us to work on enhancing the underwater image in real-time environments.

The magnitudes of absorption and scattering and the attenuation coefficients for clear water, coastal water, and harbor water for a 530-nm wavelength source is given in [2]. Optical data transmission using the non-line-of-sight link in turbid water is given in [10] along with the corresponding performances in clean water and skimmed milk (for particle diameters ranging from 10nm to 600nm) mediums. The transmission and reception of text data information along a 3-m underwater optical wireless communication (UWOC) link is shown in [11,29]. Here, the received optical beam undergoes scintillation effect because of the turbulence and air bubbles, which cause beam intensity fluctuations; therefore, errors occur in the received data. An experimental demonstration of a high-speed data transfer UWOC link using the 16-ary quadrature amplitude modulation for the 5.4-m underwater channel is shown in [12]. A similar experimental setup is demonstrated in [13] wherein a UWOC link is used with an enhanced length of 34.5 m with on-off keying (OOK) modulation. To enhance the data or image reception capability, suitable channel codes, amplifiers, transmit and receive diversities, and multiple input-multiple output schemes have been employed in literature. A Bose-Chaudhuri-Hocquenghem code augmented with the receiver diversity employed to mitigate the effects of the turbulence and turbidity is described in [14,28]. In [8], the authors show underwater image enhancement using the color channel transfer-based adaptive attenuation-curve prior approach for smoothing the light and refining the image using the saturation constraints of red, green, and blue colors. Color fusion and integrate model based underwater image enhancement techniques are shown in [15,16], respectively.

The image enhancement techniques proposed in literature are preprocessing techniques that use the color channel transfer technique; however, in this paper, we have used real-time image processing filters based on the noise observed in the received image for the OOK and binary phase-shift keying (BPSK) modulation techniques. To understand the wireless communication behavior, the bit error rate (BER) metric of the proposed system was evaluated for both the modulation schemes. BER specifies the number of information (data) bits that are in error for the transmitted information bits at a specific power. In addition to BER, the structural similarity index (SSI) and peak signal-to-noise ratio (PSNR) were used to evaluate the quality of the received image. We evaluated BER, PSNR, and SSI metrics using the OOK and BPSK modulation techniques with and without filters. The major contributions of this paper are as follows:

- The underwater optical image data transmission system has been evaluated in the presence of turbulence and beam attenuation for 50-m and 100-m UWOC channels with pure seawater, clear ocean water, and coastal ocean water as the underwater mediums.
- Studied the various levels of noise in the received image, which is arises due to the underwater turbulence and beam attenuation effects.
- The received data was processed through the real-time nonlinear filters, such as the median and corresponding associate filters, for enhancing the image quality.
- The BER performance of the proposed system with and without filters was evaluated using the OOK and BPSK modulation techniques.
- In addition to BER, we evaluated the image quality metrics, such as PSNR and SSI, for the unfiltered, median, and adaptive median-filtered responses.

Ⅱ. SYSTEM and CHANNEL MODELS

For the system and channel models for underwater image data transmission, we used an optical wireless link in an underwater turbulence medium under beam attenuation.

2.1 System model

In this research, we considered underwater image transmission using an optical wireless link of 530-nm wavelength LASER source modulated using the OOK and BPSK schemes and subject to underwater turbulence and beam attenuation effects. Fig. 1 shows the system model of the proposed underwater image data transmission system. Modulation is a way of communicating information bits in a wireless medium; it plays a crucial role in data transmission. In typical OOK modulation, the binary data '1' is transmitted with the LASER beam, whereas for the binary data '0' no beam is transmitted to the detector at the receiver end; this phenomenon is popularly known as intensity modulation. OOK modulation is commonly used for optical wireless communication links because it is inexpensive and less complex. However, the coherent modulation in the optical wireless communication system increases the receiver sensitivity, and information can be recovered from the amplitude, phase, and polarization of the incoming signal; this greatly increases the spectral efficiency as compared with the intensity modulation at a given baud rate [17,18]. Therefore, we have considered coherent BPSK and OOK modulation techniques in this paper. The data received at the photo-diode (PD) is given as [1],

$$Y = hs + n \tag{1}$$

where h is the underwater optical channel coefficient due to the underwater turbulence and

beam attenuation, s represents either OOK or BPSK modulated signal of input signal X and n is additive white Gaussian noise with zero mean and σ^2 variance. The source for the noise variance is the variance due to the shot noise σ_s^2 and thermal noise σ_{th}^2. The instantaneous signal-to-noise ratio (SNR) is given as follows:

$$\gamma = \frac{h^2 P}{\sigma^2} \tag{2}$$

2.2 Channel model

The channel fading parameter $h = h_a h_t$, here h_a is the deterministic beam attenuation parameter, and h_t is the turbulence fading parameter. Beam absorption and scattering causes attenuation, which is obtained using the Beer-Lambert law given as [10]

$$h_a = exp(-Lc(\lambda)) \tag{3}$$

where L is the link range, and $c(\lambda)$ is the wavelength-dependent beam attenuation coefficient. Beam attenuation depends upon the type of water used; the attenuation coefficient for the green laser of wavelength $\lambda = 530\,nm$ for clear water, coastal water, and turbid ocean water are given in [9].

The probability density function (PDF) associated with weak oceanic underwater turbulence was realized using the log-normal density function given as follows [19]:

$$f_{h_t}(h_t) = \frac{1}{h_t\sqrt{2\pi\sigma_X^2}} exp\left(-\frac{(\ln(h_t)-\mu_X)^2}{2\sigma_X^2}\right) \tag{4}$$

where μ_X and σ_X^2 are the mean and variance of the normal random variable $I = \ln(h_t)$. Normalized PDF obtained using $\mu_X = -\frac{\sigma_X^2}{2}$ and σ_X^2 can be obtained by equating the variance of Eq. (4) with the scintillation index (SI) given in [20]. The variance of Eq. (4), that is, $\sigma_I^2 = (exp(\sigma_X^2) - 1)$, shows the turbulence strength. The expression of SI for a plane wave can be obtained using [20] as follows:

$$\sigma_I^2 = 8\pi^2 k^2 L \int_0^1 \int_0^\infty K\Phi(K)\left(1-\cos\left(\frac{L\xi}{k}\right)\right) dK d\xi \tag{5}$$

where $k = \frac{2\pi}{\lambda}$, $\lambda = 447\,nm$ is the laser source wavelength, L is the underwater link range, and

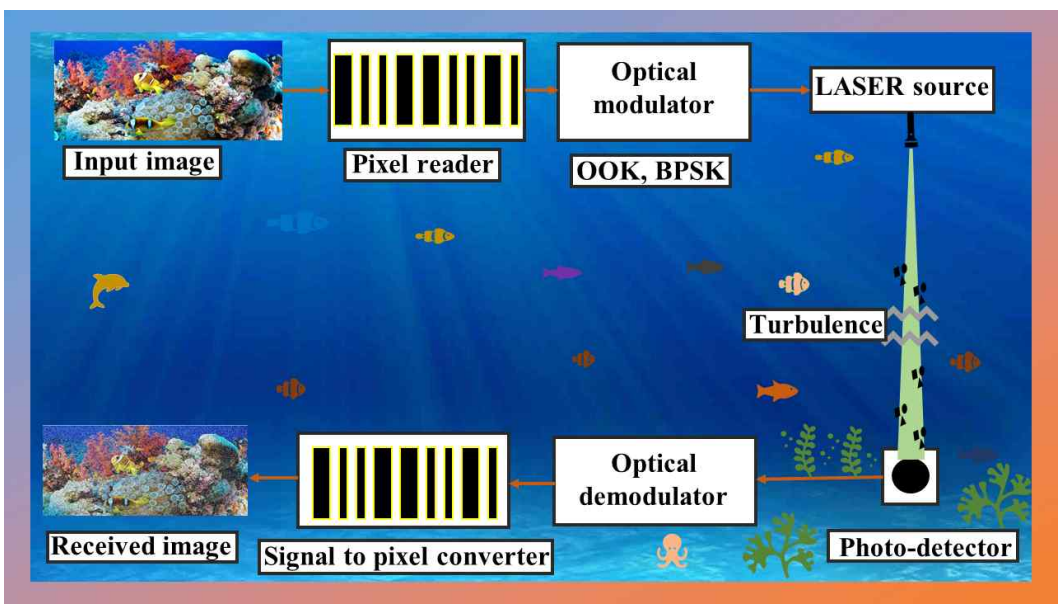

Fig. 1. Underwater wireless optical communication system model.

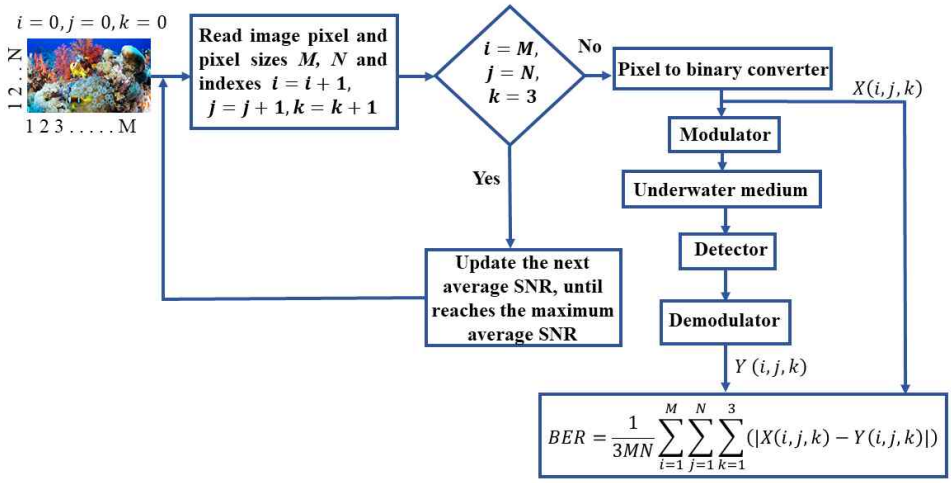

Fig. 2. Flowchart for the BER evaluation.

$\Phi(K)$ is the power spectrum of the oceanic turbulent water as [21],

$$\Phi(K)=0.388\times10^{-8}[1+2.35(K\xi)^{2/3}] \left(\omega^2 e^{-A_T\delta}+e^{-A_S\delta}-2\omega e^{-A_{TS}\delta}\right)\frac{K^{-11/3}\chi_T\epsilon^{-1/3}}{\omega^2} \quad (6)$$

where $\delta=8.284(K\xi)^{4/3}+12.978(K\xi)^2$, ϵ is the turbulence kinetic energy dissipation rate (m^2/s^3), χ_T is the dissipation rate temperature and salinity (K^2/s), ω is a unitless relative varying temperature-salinity parameter, $\xi=10^{-3}m$ is the Kolmogorov microscale length, $A_T=1.863\times10^{-2}$, $A_s=1.9\times10^{-4}$, $A_{TS}=9.41\times10^{-3}$.

The channel fading parameter $h=h_a h_l$, the corresponding PDF is obtained $f_h(h)=\left(f_{h_l}(h/h_a)\right)/h_a$ is given as,

$$f_h(h)=\frac{1}{h\sqrt{2\pi\sigma_X^2}}exp\left(-\frac{\left(\ln\left(\frac{h}{h_a}\right)-\mu_X\right)^2}{2\sigma_X^2}\right) \quad (7)$$

From the relationship given in Eq. (2), the PDF in terms of SNR obtained using,

$$f_\gamma(\gamma)=\frac{1}{2\sqrt{\gamma\bar{\gamma}}}f_h\left(\sqrt{\frac{\gamma}{\bar{\gamma}}}\right) \quad (8)$$

Expressing the overall PDF in terms of SNR as,

$$f_\gamma(\gamma)=\frac{1}{2\gamma\sqrt{2\pi\sigma_X^2}}exp\left(-\frac{\left(\ln\left(\frac{\gamma}{h_a\bar{\gamma}}\right)-2\mu_X\right)^2}{8\sigma_X^2}\right) \quad (9)$$

III. SYSTEM PERFORMANCE METRICS

The proposed UWOC system performance was obtained in terms of BER, PSNR, and SSI metrics for the OOK and BPSK modulation techniques.

3.1 Bit error rate

The BER metric shows the number of information bits that are in error at the receiver end. The BER metrics for the red, green, and blue (RGB) color images can be obtained as follows:

$$BER=\frac{1}{3MN}\sum_{i=1}^{M}\sum_{j=1}^{N}\sum_{k=1}^{3}(|X(i,j,k)-Y(i,j,k)|) \quad (10)$$

where $|.|$ is the operator for the absolute value or the non-negative value; M and N are pixel sizes of the image; and X and Y are the pixel values of the transmitted and received images, respectively. A flowchart representing the BER calculation of the

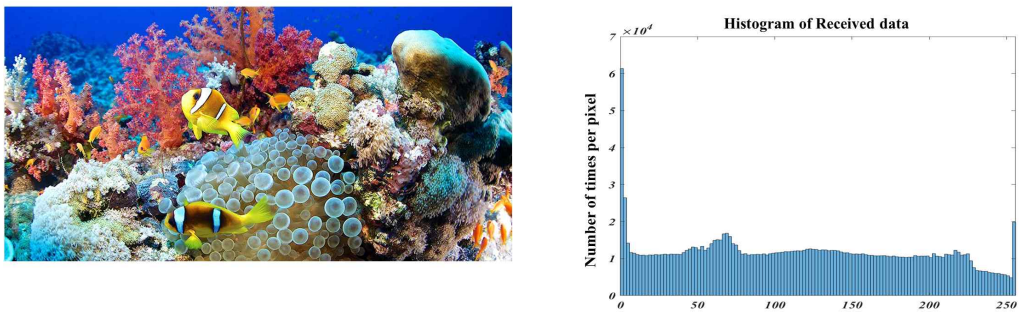

Fig. 3. Transmitted input image and corresponding histogram.

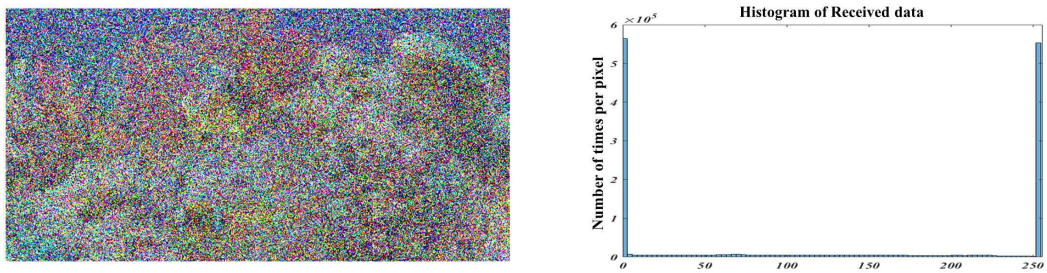

Fig. 4. On-off keying modulated received image and corresponding histogram in clear ocean water medium.

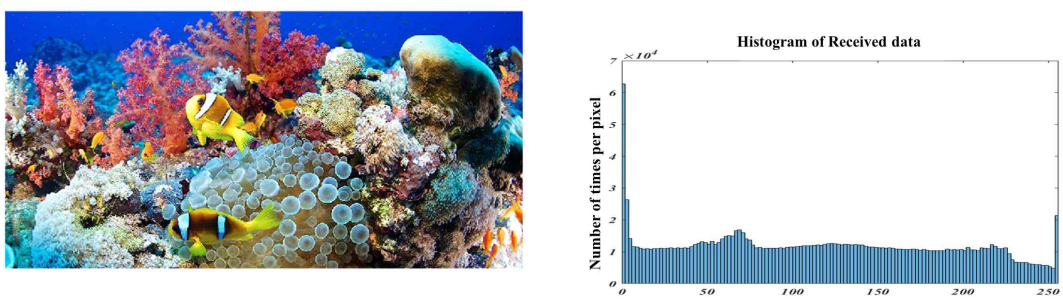

Fig. 5. Received binary phase-shift keying modulated image and corresponding histogram in clear ocean water medium

proposed system is shown in Fig. 2. Captured underwa ter image is converted into pixels using pixel reader, these pixels are transformed into equivalent binary bit streams. These binary data used to modulate via appropriate modulator and then communicated using the optical source in a underwater medium. The data lost due to the underwater channel will result errors in the reception, such errors are accumulated until all the captured pixels completed. After the completion of image pixels, corresponding BER evaluated for the red, green, and blue (RGB) color images and then evaluate average.

3.2 Peak signal-to-noise ratio

PSNR is used to measure the quality of the received image or video with respect to the quality of the transmitted image or video [22]. PSNR value of the reconstructed image obtained mathematically as $20\log_{10}\left(\frac{P_{\max}}{\sqrt{MSE}}\right)$, here $P_{\max}=255$ is maximum pixel

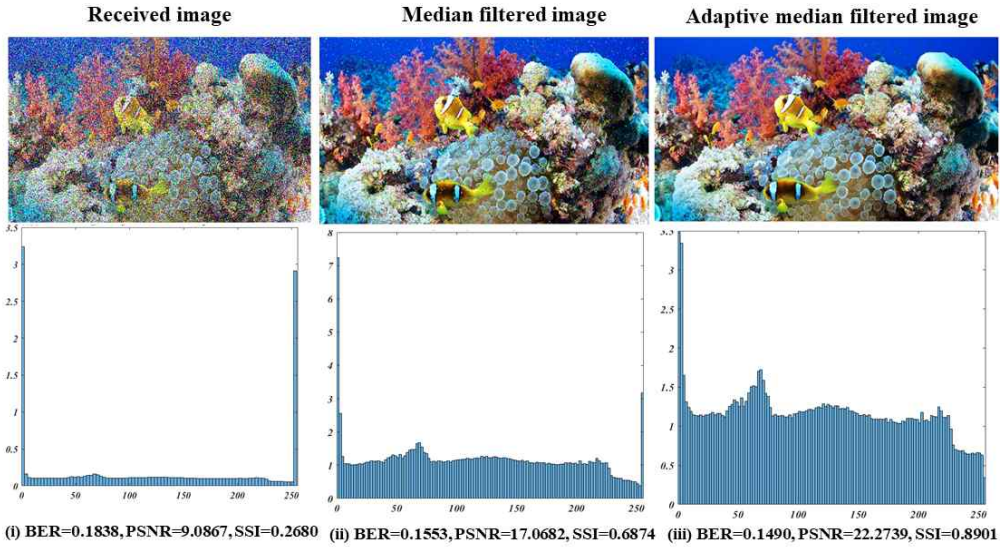

(a)

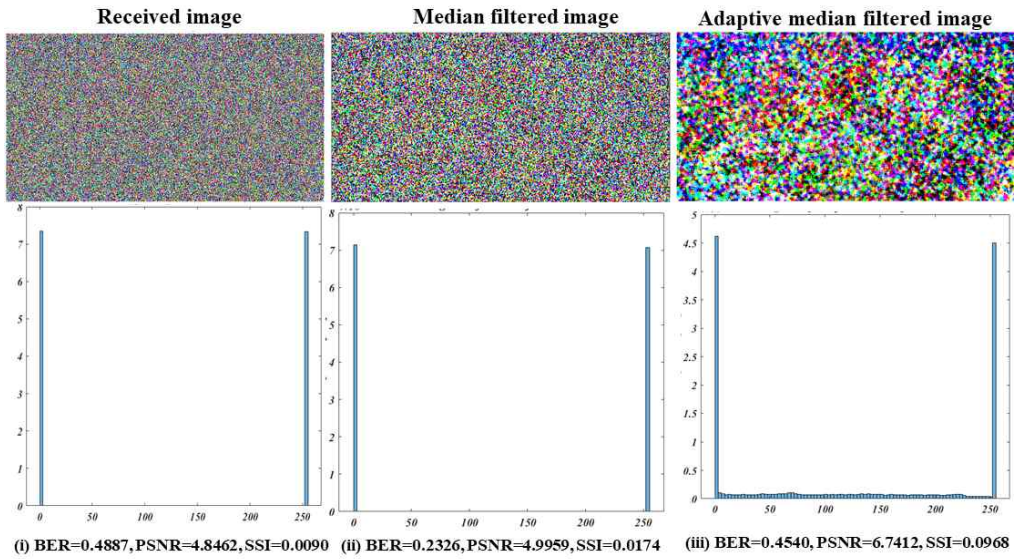

(b)

Fig. 6. On-off keying modulated received images at 10-dB average SNR and corresponding histograms for (i) UF, (ii) MF, (iii) AMF, (a) pure seawater medium, and (b) coastal ocean water medium.

value, *MSE* is mean squared error, which compares the true pixel value of the input/transmit image or video to the received/reconstructed image or video. Higher PSNR represents the received/reconstructed image has good match with the transmit/input image.

3.3 Structural similarity index

For identical transmit and received images, *MSE* is zero. Hence, PSNR will be undefined (division by zero). The main limitation of PSNR is relies strictly on numeric comparison and does not actually consider

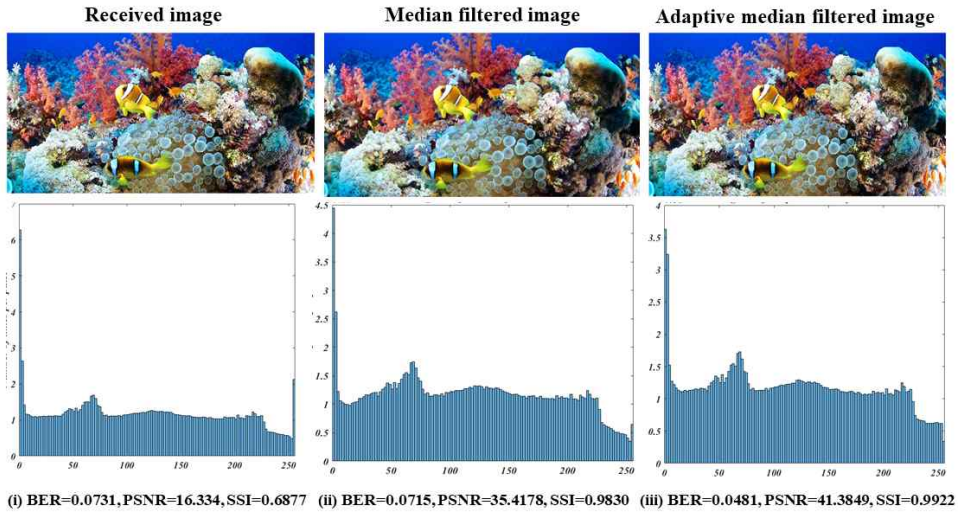

(a)

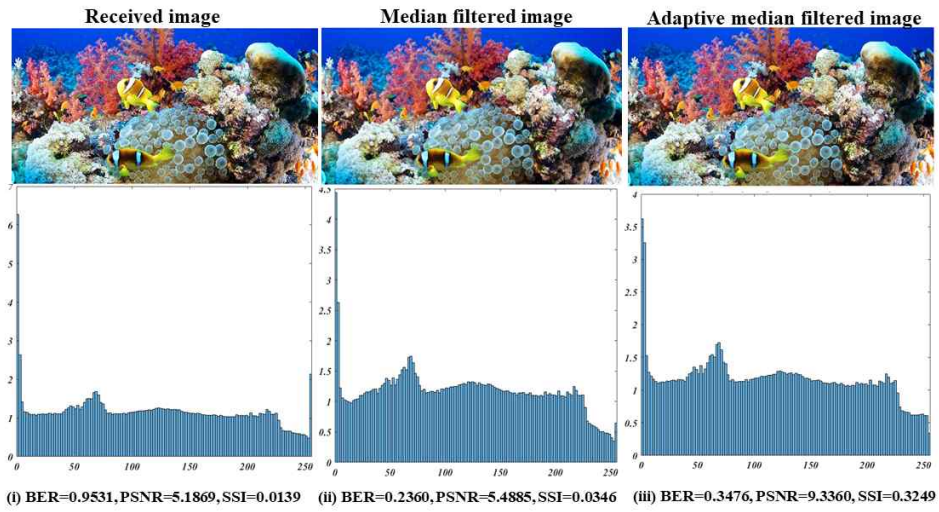

(b)

Fig. 7. Binary phase-shift keying modulated received images at 10-dB average SNR and corresponding histograms for (i) UF, (ii) MF, (iii) AMF, (a) pure seawater medium, and (b) coastal ocean water medium.

any level of biological factors of the human vision system. SSI is a popular image quality measurement metric based on human visual characteristics, which shows the similarity between the received image and the transmitted image [23]. Hence, we have evaluated the SSI for the received/reconstructed images with respect to the transmit image.

Ⅳ. RECEIVED IMAGE ENHANCEMENT USING THE MEDIAN AND CORRESPONDING ASSOCIATED FILTER

The underwater image and corresponding histogram are shown in Fig. 3. The underwater image was

transmitted via various underwater mediums in the presence of turbulence and various levels of attenuation impacts. Figs. 4 and 5 show the images received using the OOK and BPSK modulations, respectively, in the clear ocean water medium for the 50-m link at 10-dB average SNR

value. The BER, PSNR, and SSI values obtained using OOK modulation for a clear ocean water medium with 10-dB average SNR were 0.3631, 6.1277, and 0.0834, respectively. Similarly, the BER, PSNR, and SSI values obtained for the BPSK-modulated scheme operated with the same clear ocean water medium and average SNR were 0.0020, 31.7611, and 0.9848, respectively.

The received images are noisy versions of the transmitted image. This happened because the transmitted pixel values of the images were corrupted by the noisy characteristics of the underwater medium. Noise occurred because the malfunctioning pixel was a random-valued impulse noise. Researchers have circumvented this noise by employing several decision-making nonlinear filters to enhance the impulse noise images [24,25]. Median filter (MF) extensions show good improvement over the impulse noise [22,26], which partitions the input image as multiple windows and then computes the median of each window. The window having the noisy pixel is determined by using the decision-making capability and is replaced with the median pixel value of the window. However, one drawback of an MF is that it replaces the median pixel value without considering the edges of the image. An adaptive MF (AMF) was proposed by remedying the MFs and center-weighted MFs. Hence, the output pixel switched between the median pixel and current pixel values. The received images using unfilter (UF), MF, and AMF are shown with histograms in Figs. 6 and 7 for pure seawater and coastal ocean water mediums. The metrics of the received data, such as BER, PSNR, and SSI, are depicted in Section 5.

Table 1. Beam attenuation for the various underwater mediums of 50-m and 100-m length for UWOC at 530-nm wavelength source.

Water type	$c(\lambda)$	Attenuation	
		50 m	100 m
Pure sea (PW)	0.056	6.08×10^{-2}	3.70×10^{-3}
Clear ocean (CO)	0.151	5.26×10^{-4}	2.76×10^{-7}
Coastal ocean (COA)	0.399	2.16×10^{-9}	4.69×10^{-18}

V. RESULTS AND DISCUSSIONS

Beam absorption, scattering and attenuation coefficients of different turbid underwater mediums are obtained in [27], whereas in this paper, the beam absorption, scattering, and attenuation coefficients for the various underwater mediums are given in Table 1.

Fig. 8 shows a comparison of the images received using various techniques, such as OOK and BPSK modulation and UF, MF, and AMF filtering. Fig. 8 also shows the images received for clear ocean water, pure seawater, and coastal ocean water for links that are 50-m and 100-m long for average SNRs of 10dB, 5dB, and 15dB. The average SNRs are with reference to the unfiltered OOK-modulated UWOC in the 50-m long clear ocean water medium operated at the average SNR of 10dB. Enhanced image quality was observed from UF to MF and AMF, and there was an increase in the average SNRs from 5dB to 10dB and 15dB. Variation in image quality was observed from OOK to BPSK modulation and from pure seawater to clear ocean water and coastal ocean water mediums.

Fig. 9 shows the BER performance of the proposed

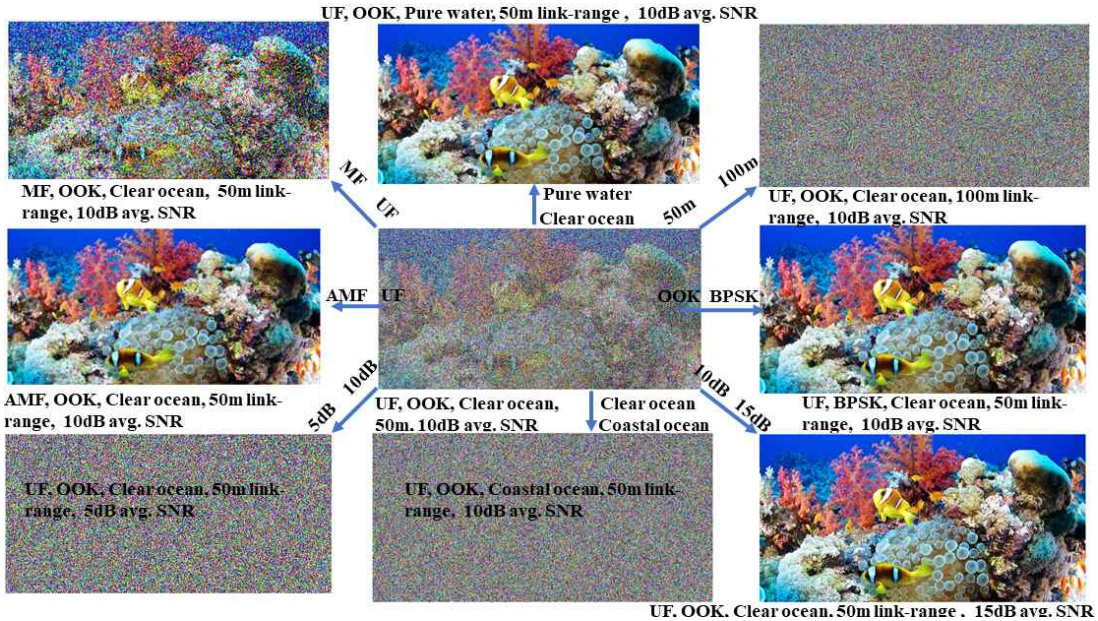

Fig. 8. Received image comparison using the various proposed techniques.

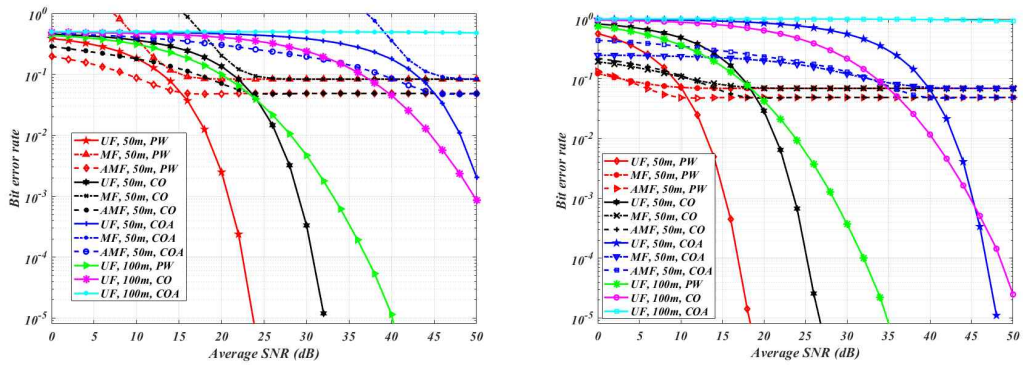

(a) (b)

Fig. 9. Bit error rate (a) OOK and (b) BPSK.

system under the influence of pure seawater, clear ocean water, and coastal ocean water as mediums with and without filters for the OOK and BPSK modulation schemes with links that were 50-m and 100-m long. Fig. 9a and 9b show the BER performance of the OOK modulated scheme, and the BPSK-modulated scheme, respectively. The UF has achieved up to 1×10^{-5} BER performance, whereas an error floor (A phenomena of obtaining the same BER with the increment of average SNR) was observed in the BER performances of MF and AMF; this was because the filter masked the median pixel value rather than the exact pixel value of the corrupted window pixel. Hence, image improvement could be observed rather than improvement in the exact information bits.

Therefore, we evaluated the SSI and PSNR performances in addition to the BER performance. For the UF system, we obtained 1.5×10^{-5} BER for pure seawater, clear ocean water, and coastal ocean water

mediums at average SNR values of 23dB, 31dB, and more-than-50-dB, respectively. This implies that varying the medium from pure seawater to clear ocean water and coastal ocean water caused 7dB and more-than-20-dB average performance deterioration, respectively, because of the increase in attenuation at 1.5×10^{-5} BER. Similarly, for the 50-m link UWOC system operated in the presence of pure seawater medium, we obtained 1×10^{-5} BER at the average SNR of 24dB, whereas for the 100-m link UWOC system of the same medium, we obtained the same performance at the average SNR value of 40dB. Hence, the variations in the link length from 50-m to 100-m caused a performance deterioration of 16dB at 1×10^{-5} BER. Figs. 9a and 9b show that the BPSK-modulated system gained an average SNR value of 5dB when compared with the OOK-modulated system.

respectively. The maximum PSNR value is the maximum image-enhanced capacity of the specified method (with or without filter), which means that the received image pixels are unchanged after the specific average SNR. From Fig. 10a, for the pure seawater medium of the 50-m UWOC link using UF, MF, and AMF with the average SNR value of 20dB, we obtained PSNR values of 28.039, 38.450 and 43.259, respectively. For the 50-m UWOC link with unfiltered pure seawater, clear ocean water, and coastal ocean water, we obtained a PSNR performance of 28.50 for average SNR values of 20dB, 28.50dB, and 50dB. For the 50-m UWOC links with the median-filtered pure seawater, clear ocean water, and coastal ocean water mediums, we obtained the same PSNR performance at average SNR values of 13dB, 21dB, and 43dB. For 50-m UWOC mediums of adaptive median-filtered pure seawater, clear ocean water, and coastal ocean water, we obtained

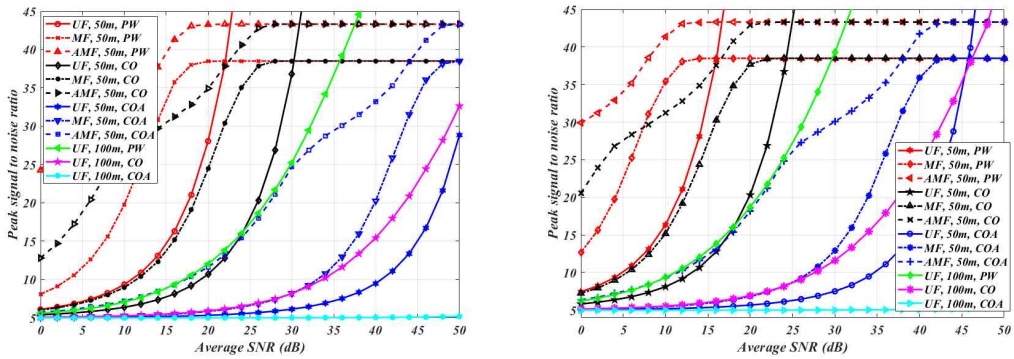

(a) (b)

Fig. 10. Peak signal-to-noise ratio obtained using (a) OOK and (b) BPSK.

Fig. 10 shows the PSNR variations of the UF, MF, and AMF UWOC system for the pure seawater, clear ocean water, and coastal ocean water mediums of 50-m and 100-m lengths. Figs. 10a and 10b are the PSNR plots for the OOK and BPSK modulation techniques, respectively. PSNR indicates the quality of the received image; a high PSNR value shows a good image quality. Figs. 10a and 10b show that the maximum PSNR values of AMF, MF, and UF responded images are 43.314, 38.497, and 45,

the same PSNR performance for average SNR values of 4dB, 12dB, and 34dB, respectively. Similarly, we compared the unfiltered pure seawater, clear ocean water, and coastal ocean water mediums for 50-m and 100-m links. For 50-m unfiltered pure seawater and clear ocean mediums, we obtained a PSNR value of 32.50 at 20.50dB and an average SNR of 27dB. For the 100-m link, we obtained PSNR values of 33dB and 5dB, respectively, for the pure seawater and clear ocean water mediums. The PSNR value of the 100-m

link in the coastal ocean medium was approximately 5 at 50-dB average SNR, whereas the same average SNR for the 50-m coastal ocean UWOC link gave a PSNR value of 28.837. The similar comparisons can be obtained for the BPSK-modulated system shown in Fig. 10b.

Fig. 11 shows the SSI variations of UF, MF, and AMF UWOC systems for the pure seawater, clear ocean water, and coastal ocean water mediums of 50-m and 100-m lengths. Figs. 11a and 11b are the SSI plots for the OOK and BPSK modulation techniques, respectively. When the SSI value approached one, the degree of similarity between the received image and the transmitted image became negligible. For a 50-m OOK modulated unfiltered UWOC link, we obtained unity SSI at 20-dB average SNR. However, for the median at 12dB and the adaptive median-filtered system at 6dB, respectively, we obtained the same SSI value. For the 50-m UWOC link, the unfiltered pure seawater medium reached unity SSI at 20dB, whereas for the clear ocean water and coastal ocean water mediums, we obtained the same SSI at 30 and 50dB, respectively. For the 50-m and 100-m links with pure seawater medium, we obtained unity SSI at 20dB and 30dB, respectively. Similarly, the 50-m and 100-m links reached unity SSI using the clear ocean water medium at 30-dB and 50-dB average SNRs, respectively, and 0.014 SSI using the coastal ocean water medium at 16-dB and 50-dB average SNRs. A similar performance comparison can be done using the BPSK-modulated UWOC system SSI performance, as shown in Fig. 11b.

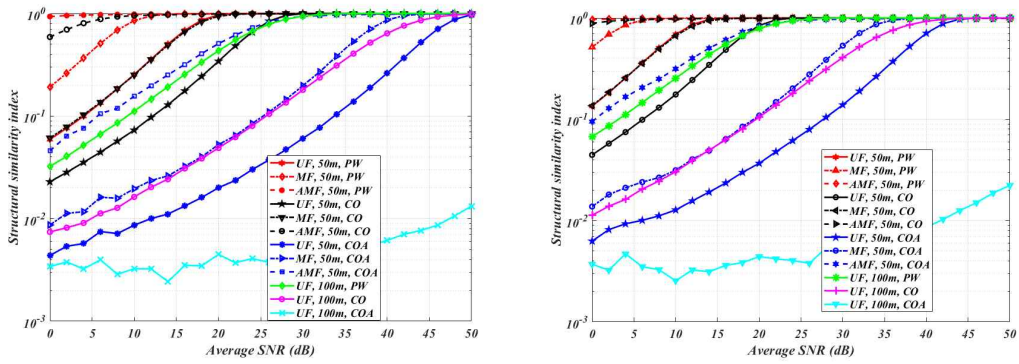

(a) (b)

Fig. 11. Structural similarity index for (a) OOK and (b) BPSK.

VI. CONCLUSIONS

This paper demonstrates the BER, PSNR, and SSI performances for underwater image data transmission with underwater turbulence and beam attenuation in different water mediums, namely, pure seawater, clear ocean water, and coastal ocean water. The results of the proposed system were obtained using the OOK and BPSK modulation techniques for 50-m and 100-m UWOC links, respectively. Based on the noise in the received image, we employed MFs and AMFs to enhance the image quality. In this paper, we have shown the BER, PSNR, and SSI performance results for MFs and AMFs with respect to the average SNR. Error floor in the BER responses of the MF and AMF are indicates that the filters are poor at estimating the exact information bits rather than estimating the received image. Hence, PSNR and SSI indicates the similarity of the received MF and AMF responded images with the transmitted image for the varying the average SNR.

ACKNOWLEDGMENTS

This research work was supported by a Research Grant of Pukyong National University (2021).

REFERENCES

[1] Naik, R. P., Simha, G. G., & Krishnan, P. (2021). Wireless-optical-communication-based cooperative IoT and IoUT system for ocean monitoring applications. Applied Optics, 60(29), 9067-9073.

[2] Hanson, F., & Radic, S. (2008). High bandwidth underwater optical communication. Applied optics, 47(2), 277-283.

[3] Kumar, L. B., Ramavath, P. N., & Krishnan, P. (2022). Performance analysis of multi-hop FSO convergent with UWOC system for security and tracking in navy applications. Optical and Quantum Electronics, 54(6), 1-26.

[3] Naik, R. P., Acharya, U. S., Lal, S., & Krishnan, P. (2022). Performance investigation of underwater wireless optical system for image transmission through the oceanic turbulent optical medium. Optical and Quantum Electronics, 54(4), 1-16.

[5] Kaushal, H., & Kaddoum, G. (2016). Underwater optical wireless communication. IEEE access, 4, 1518-1547.

[6] Mohan, S., & Simon, P. (2020). Underwater image enhancement based on histogram manipulation and multiscale fusion. Procedia Computer Science, 171, 941-950.

[7] Ramavath, P. N., Udupi, S. A., & Krishnan, P. (2020). High-speed and reliable underwater wireless optical communication system using multiple-input multiple-output and channel coding techniques for IoUT applications. Optics Communications, 461, 125229.

[8] Liu, K., & Liang, Y. (2021). Underwater image enhancement method based on adaptive attenuation-curve prior. Optics express, 29(7), 10321-10345.

[9] Levidala, B. K., Ramavath, P. N., & Krishnan, P. (2021). Performance enhancement using multiple input multiple output in dual-hop convergent underwater wireless optical communication-free-space optical communication system under strong turbulence with pointing errors. Optical Engineering, 60(10), 106106.

[10] Pan, Z., Xiao, Y., Zhou, L., Cao, Y., Yang, M., & Chen, W. (2021). Non-line-of-sight optical information transmission through turbid water. Optics Express, 29(24), 39498-39510.

[11] Ramavath, P. N., Kumar, A., Shashikant Godkhindi, S., & Acharya, U. S. (2018). Experimental studies on the performance of underwater optical communication link with channel coding and interleaving. Csi Transactions on Ict, 6(1), 65-70.

[12] Oubei, H. M., Duran, J. R., Janjua, B., Wang, H. Y., Tsai, C. T., Chi, Y. C., ... & Ooi, B. S. (2015). 4.8 Gbit/s 16-QAM-OFDM transmission based on compact 450-nm laser for underwater wireless optical communication. Optics express, 23(18), 23302-23309.

[13] Liu, X., Yi, S., Zhou, X., Fang, Z., Qiu, Z. J., Hu, L., & Tian, P. (2017). 34.5 m underwater optical wireless communication with 2.70 Gbps data rate based on a green laser diode with NRZ-OOK modulation. Optics express, 25(22), 27937-27947.

[14] Ramavath, P. N., Udupi, S. A., & Krishnan, P. (2020). Experimental demonstration and analysis of underwater wireless optical communication link: Design, BCH coded receiver diversity over the turbid and turbulent seawater channels. Microwave and Optical Technology Letters, 62(6), 2207-2216.

[15] Ancuti, C. O., Ancuti, C., De Vleeschouwer, C., & Bekaert, P. (2017). Color balance and fusion for underwater image enhancement. IEEE Transactions on image processing, 27(1), 379-393.

[16] Iqbal, K., Salam, R. A., Osman, A., & Talib, A. Z. (2007). Underwater Image Enhancement Using an Integrated Colour Model. IAENG International Journal of computer science, 34(2).

[17] Cvijetic, N., Qian, D., Yu, J., Huang, Y. K., & Wang, T. (2010). Polarization-multiplexed optical wireless transmission with coherent detection. Journal of Lightwave Technology, 28(8), 1218-1227.

[18] Fried, D. L. (1967). Optical heterodyne detection of an atmospherically distorted signal wave front. Proceedings of the IEEE, 55(1), 57-77.

[19] Vali, Z., Gholami, A., Ghassemlooy, Z., Omoomi, M., & Michelson, D. G. (2018). Experimental study of the turbulence effect on underwater optical wireless communications. Applied optics, 57(28), 8314-8319.

[20] Korotkova, O., Farwell, N., & Shchepakina, E. (2012). Light scintillation in oceanic turbulence. Waves in Random and Complex Media, 22(2), 260-266.

[21] Ata, Y., & Baykal, Y. (2014). Scintillations of optical plane and spherical waves in underwater turbulence. JOSA A, 31(7), 1552-1556.

[22] Naik, R. P., Acharya, U. S., Lal, S., & Krishnan, P. (2022). Performance investigation of underwater wireless optical system for image transmission through the oceanic turbulent optical medium. Optical and Quantum Electronics, 54(4), 1-16.

[23] Wang, Z., & Bovik, A. C. (2002). A universal image quality index. IEEE signal processing letters, 9(3), 81-84.

[24] Lin, H. M., & Willson, A. N. (1988). Median filters with adaptive length. IEEE transactions on circuits and systems, 35(6), 675-690.

[25] Sun, T., & Neuvo, Y. (1994). Detail-preserving median based filters in image processing. Pattern recognition letters, 15(4), 341-347.

[26] Garnett, R., Huegerich, T., Chui, C., & He, W. (2005). A universal noise removal algorithm with an impulse detector. IEEE Transactions on image processing, 14(11), 1747-1754.

[27] Uppalapati, A., Naik, R. P., & Krishnan, P. (2020). Analysis of M-QAM modulated underwater wireless optical communication system for reconfigurable UOWSNs employed in river meets ocean scenario. IEEE Transactions on Vehicular Technology, 69(12), 15244-15252.

[28] Salman, J. Bolboli and W. -Y. Chung, "Experimental Demonstration and Evaluation of BCH-Coded UWOC Link for Power-Efficient Underwater Sensor Nodes," in IEEE Access, vol. 10, pp. 72211-72226, 2022, doi: 10.1109/ACCESS.2022.3188247.

[29] Maaz Salman, Javad Balboli, Ramavath Prasad Naik, W.-Y. Chung and J.-J. Kim. "Aqua-Aware: Underwater Optical Wirelesss Communication enabled Compact Sensor Node, Temperature and Pressure Monitoring for Small Moblie Platforms", Journal of the Institute of Convergence Signal Processing, 23(2), pp. 50-61, 2022

저자소개

Ramavath Prasad Naik

2012년 : Jawaharlal Nehru Technology University, India 전기통신공학부(공학사)
2015년 : Motilal Nehru National Institute of Technology, India Allahabad, Uttar Pradesh 전기통신공학부(공학석사)
2021년 : National Institute of Engineering, Mysore 조교수
2021년 : National Institute of Engineering, Mysore 조교수
2021년~현재 : 부경대학교 Postdoctoral Researcher
관심분야: Free-Space and Underwater optical wireless communication, Theory and application of error control codes and Co-operative communication

MAAZ SALMAN

2018년 : 파키스탄 공과대학교 전기통신정보공학부(공학 학사)
2020년 : 순천향대학교 전기전자공학부(공학 석사)
2020년~현재 : 부경대학교 인공지능융합학과 박사과정
관심분야: 수중 사물 인터넷, 수중 광무선 통신, 인공지능, 센서 네트워크.

정 완 영 (WAN-YOUNG CHUNG)

1987년 : 경북대학교 전자공학과(공학사)
1989년 : 경북대학교 전자공학과(공학석사)
1998년 : 큐슈대학교 센서공학(공학박사)
1999년~2008년 : 동서대학교 부교수
현재 : 부경대학교 전자공학과 정교수
관심분야: 무선 센서 네트워크, 유비쿼터스 의료 및 자동차 응용 프로그램, 가시광선 통신이 가능한 스마트 발광 시스템, 임베디드 시스템